Biome-specific fire emission rates of NO_x from MODIS and GOME-2/OMI satellite-derived data sets

Stefan F. Schreier[1*], Andreas Richter[1], Johannes W. Kaiser[2], and John P. Burrows[1]

[1] Institute of Environmental Physics/Remote Sensing, University of Bremen, Germany

[2] King's College London, UK; ECMWF, UK; MPI for Chemistry, Germany

*Email: schreier@iup.physik.uni-bremen.de

Biomass burning as a source of NO_x emissions

Why important?

NO_x radicals play key roles in tropospheric chemistry

Nitric oxide (NO) and nitrogen dioxide (NO_2) are coupled in the atmosphere

- $NO + O_3 \rightarrow NO_2 + O_2$ — NO_2 is produced from NO by its reaction with ozone (O_3)
- $NO_2 + h\nu \rightarrow NO + O$ — NO_2 is photolyzed to produce NO and an oxygen atom (O)
- $O + O_2 + M \rightarrow O_3 + M$ — O reacts with molecular oxygen (O_2) to produce O_3
- $N_2 + O_2 = NO + NO$ — Molecular nitrogen (N_2) and O_2 participate to form NO

NO_x and O_3 are both toxic and the exposure to these hazardous gases impacts on human health

How to measure?

NO_2 amounts and distributions are retrieved by passive and active remote sensing techniques in the UV/VIS, near IR, IR, and microwave regions

ground based, ship and aircraft borne, satellite based Differential Optical Absorption Spectroscopy (DOAS)

How to estimate globally?

bottom-up approach: aggregate divers local statistics

burned area, fuel load, combustion completeness, emission factor

top-down approach: using atmospheric understanding

inversion and partitioning of satellite-derived tropospheric NO_2 columns

Estimation of fire emission rates of NO_x

1. Temporal correlation between fire radiative power (FRP) and tropospheric NO_2 vertical columns (TVC NO_2)

- Monthly means of FRP are analyzed for temporal correlation with monthly means of TVC NO_2
- 5 consecutive years from 2007 to 2011
- 1° x 1° grid (to overcome the effects of horizontal transport of NO_2)
- Globally and for characteristic biomass burning regions

The aims of the study

To establish an empirical relationship between FRP and TVC NO_2 as a tool to estimate fire emissions of NO_x. The correlation of FRP and TVC NO_2 is studied globally and for selected regions, and fire emission rates (FERs) for a total of 11 different types of vegetation are derived for the morning (early afternoon) by making use of the linear relationship between MODIS Terra (Aqua) FRP and TVC NO_2 from GOME-2 (OMI) over characteristic biomass burning regions.

2. Conversion of TVC NO_2 into NO_x emissions and comparison with bottom-up NO_x emissions

$$P = TVC[NO_2] \ast M \ast [NO_2]/[NO] \ast A_b \,/\, NA \ast \tau \qquad [\text{g } NO_x \text{ s}^{-1}]$$

P … production rate of NO_x, M … molar mass of NO_x, $[NO_2]/[NO] = 0.6$, A_b … pixel area, NA … Avodagro's number, τ … lifetime of NO_x, assumed to be 8 hours (GOME-2) and 4 hours (OMI)

- Pixel-wise subtraction of y-intercepts for removing 'background'
- Comparison of estimated NO_x emissions with GFED3.1 database

3. Fire emission rates (FERs) of NO_x

- Inclusion of a global land cover map for biome-specific analysis
- Inclusion of a population density data set for exclusion of strongly anthropogenically influenced 1° x 1° boxes
- Estimation of fire emission rates by computing the best fitting least-squares regression lines for each land cover type using all 1° x 1° boxes having r > 0.3 and population density < 100 persons km^{-2}

Instruments and data retrieval

Global Ozone Monitoring Experiment-2 (GOME-2)

- on board MetOp-A (EUMETSAT) since October 2006
- spectral range: 240-790 nm at 0.2-0.4 nm resolution
- pixel size in nadir-viewing geometry: 80 x 40 km^2
- local equatorial crossing time: 9:30 a.m.

Ozone Monitoring Instrument (OMI)

- on board EOS-Aura (NASA) since July 2004
- 270-500 nm at 0.63 nm spectral resolution
- 13 x 24 km^2 at nadir point
- local equatorial crossing time: 1:30 p.m.

Retrieval of tropospheric NO_2 vertical columns (TVC NO_2)

1. Differential Optical Absorption Spectroscopy (DOAS) for retrieving the slant column densities (SCDs) spectral fitting window: 425-497 nm (GOME-2), see Richter et al. (2011) and 405-465 nm (OMI), see Bucsela et al. (2006)
2. The reference sector method is used for removing the stratospheric part from the NO_2 SCDs
3. Pixel-wise measurements with cloud fraction > 0.2 are removed (using FRESCO+)
4. Tropospheric SCDs are converted into tropospheric vertical columns (**TVC NO_2**) by using airmass factors (AMFs)

MODerate resolution Imaging Spectroradiometer (MODIS)

- on board Terra (10:30 a.m.) and Aqua (1:30 p.m.) satellites (NASA), 36 spectral bands ranging from 0.4-14.4 µm
  differences in 4- and 11-um black body radiation are used to derive active fires at 1 km^2 horizontal resolution
  the MODIS fire products additionally offer the radiant component of energy release, the so-called fire radiative power (**FRP**)

1. Temporal correlation between fire radiative power and tropospheric NO_2 columns

Fig.1: Global mean tropospheric NO_2 vertical columns (2007-2011) retrieved from GOME-2 measurements

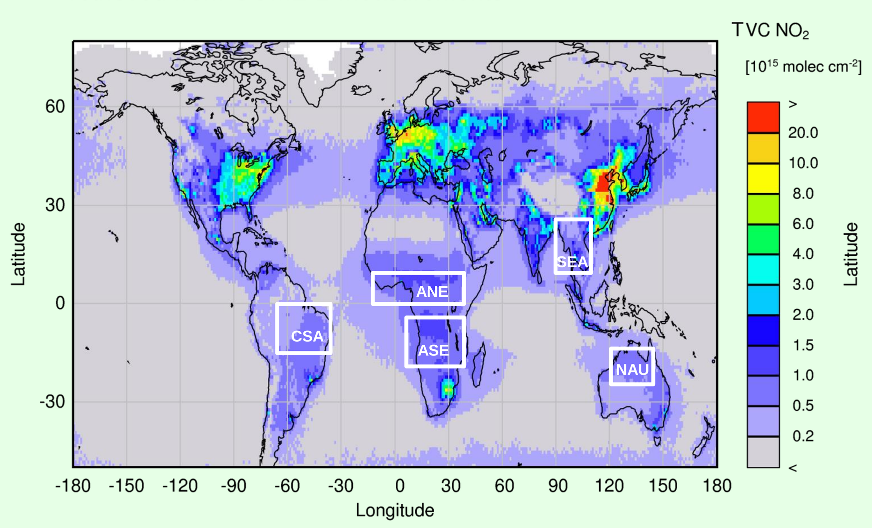

Fig.2: Correlation coefficients describing the temporal relationship (2007-2011) between FRP (Terra MODIS) and TVC NO_2 (GOME-2)

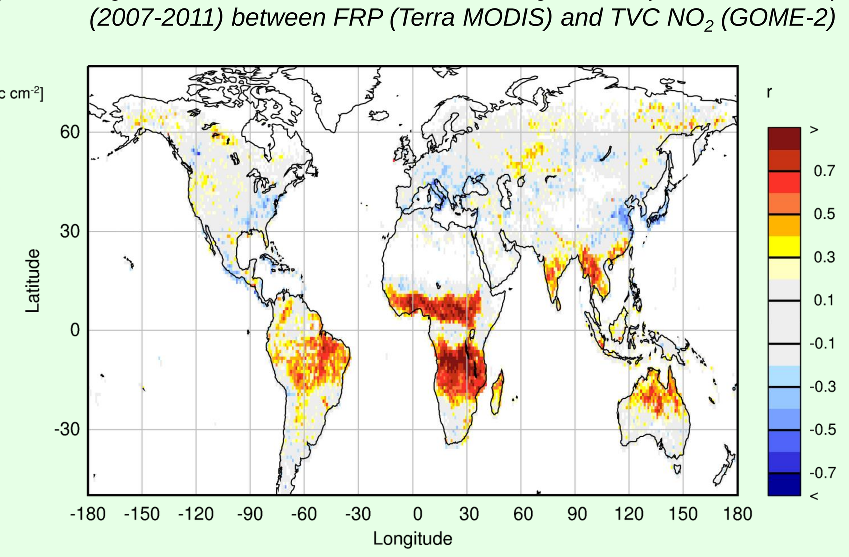

Fig. 3: Temporal variability of MODIS Terra (red) and Aqua (orange) derived FRP (monthly means) and GOME-2 (turquois) and OMI (blue) derived TVC NO_2 (monthly means)

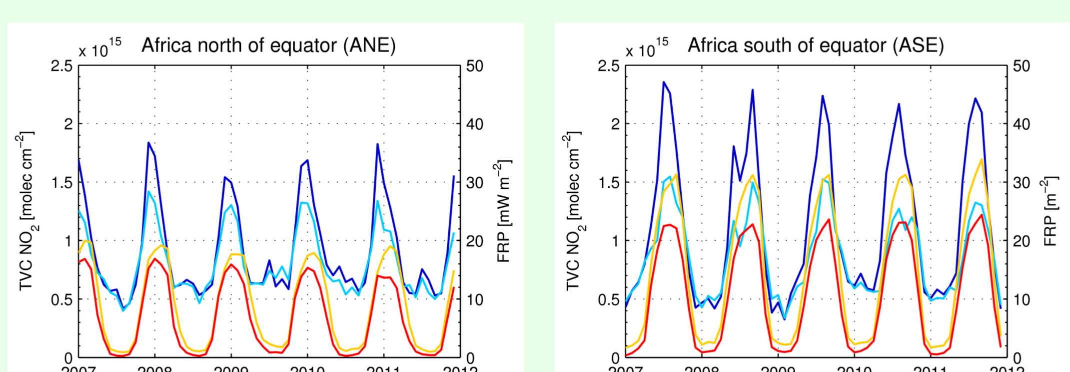

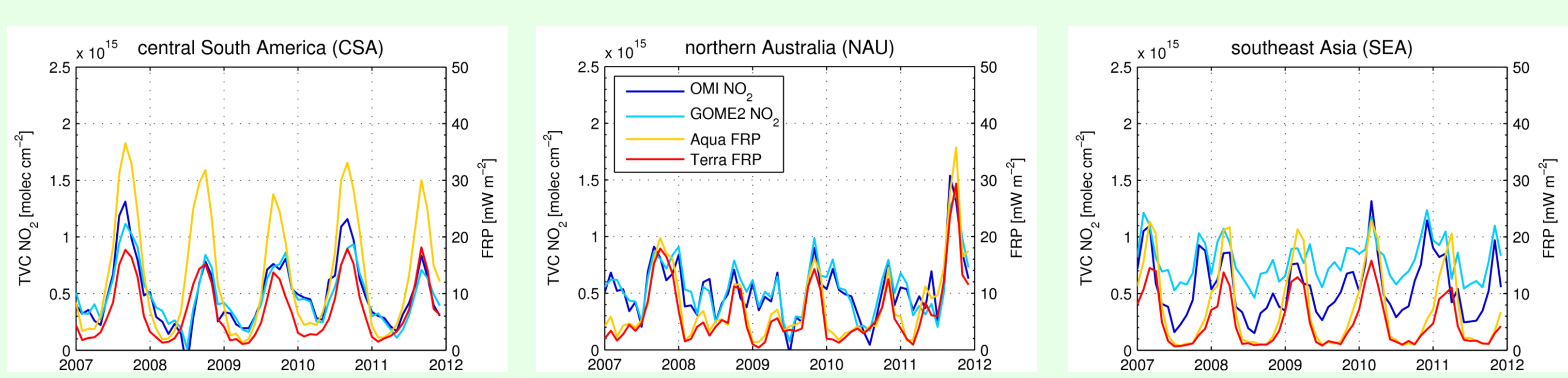

The highest correlation coefficients of r > 0.8 are found in Africa, south of the equator (ASE) and north of the equator (ANE).

Moderate to high correlation coefficients are also apparent in central South America (CSA), northern Australia (NAU), and southeast Asia (SEA).

In general, FRP and TVC NO_2 are higher during early afternoon, as indicated by MODIS Aqua and OMI observations.

2. Conversion of TVC NO_2 into NO_x emissions and comparison with bottom-up NO_x emissions

Fig. 4: Mean y-intercepts of the best fitting least-squares regression lines (2007-2011) for pixels with r > 0.3 (GOME-2 vs. MODIS Terra)

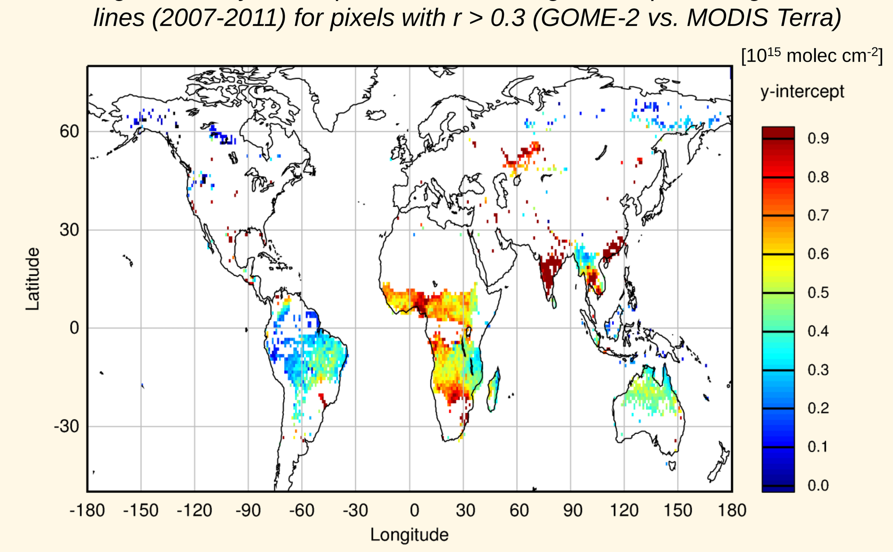

Fig. 5: Mean gradients of the best fitting least-squares regression lines (2007-2011) for pixels with r > 0.3 (GOME-2 vs. MODIS Terra)

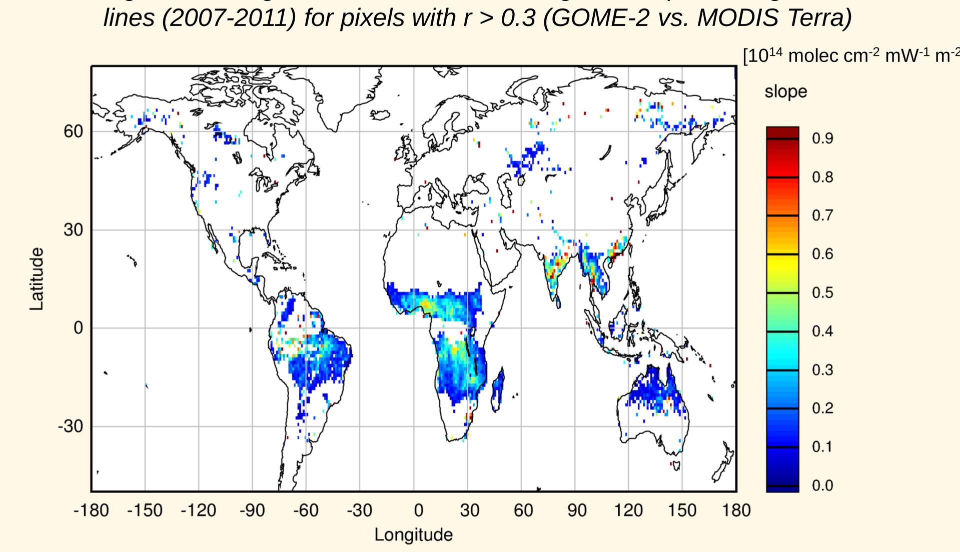

Fig. 6: Comparison between converted NO_x emission rates, retrieved from the GOME-2 (blue) and OMI (red) measurements, and GFED3.1 NO_x emission rates. Here, the lifetime of NO_x is assumed to be 8 hours (GOME-2) and 4 hours (OMI).

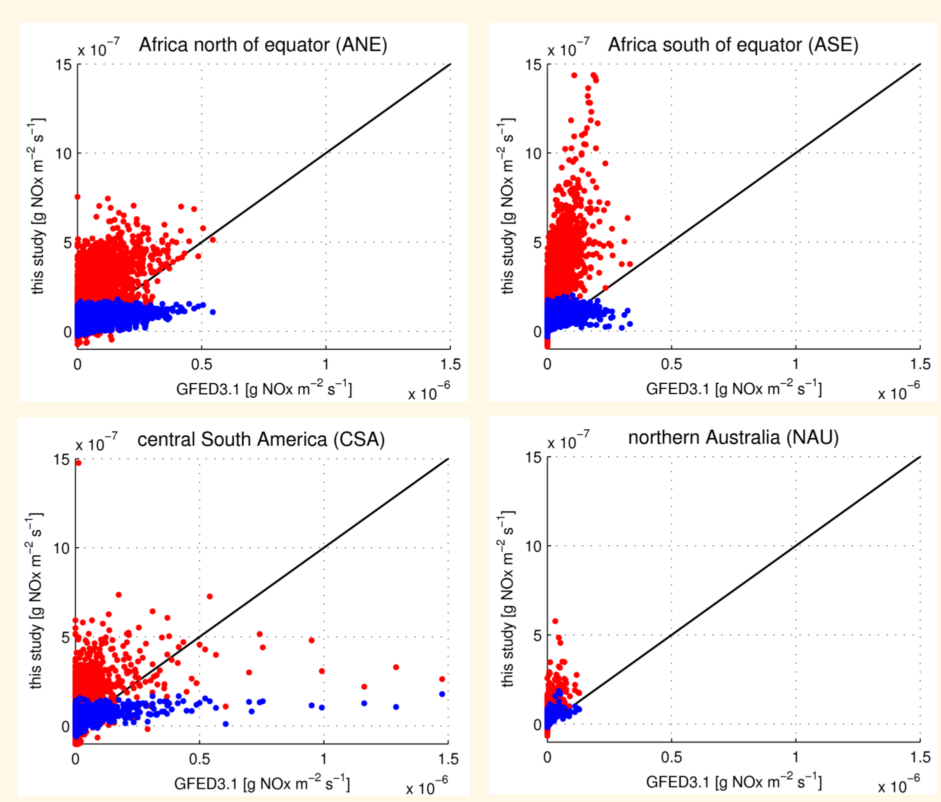

The distribution of gradients is smooth and shows only moderate variation, indicating that a robust link exists between FRP and TVC NO_2.

High y-intercept values can be interpreted as a clear signal of NO_x emissions from other sources (e.g. anthropogenic, lightning, soil).

The comparison between GFED3.1 and NO_x emissions derived in this study indicate that emissions lay within an order of magnitude. NO_x emissions derived from satellite measurements are higher in Africa south of the equator and lower in central South America.

Fig. 7: Global land cover map (from GLCF) used for the distinction of the different land cover types (labels are shown in Table 1)

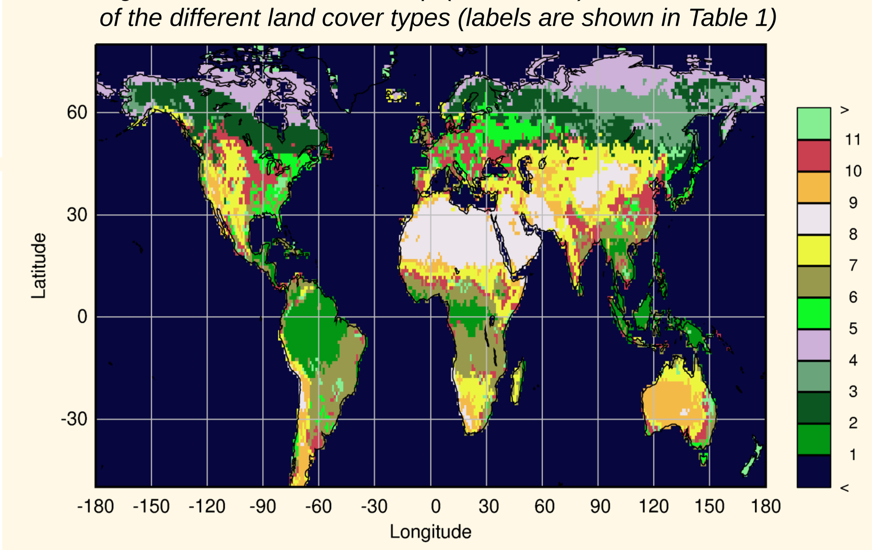

3. Fire emission rates (FERs) of NO_x

FERs of NO_x for the dominating types of vegetation burned are 1.21 (3.22), 0.77 (2.11), 1.14 (2.57), and 1.03 (1.77) g NO_x s^{-1} MW^{-1} for wooded grassland, grassland, cultivated crops, and broadleaf deciduous forest, respectively, in the morning (early afternoon)

In the case of wooded grassland, the gradients of the lines for the African regions show good agreement, whereas FERs are higher in southeast Asia and lower in central South America. Here, the lifetime for GOME-2 (OMI) is assumed to be 8 hours (4 hours).

Tab. 1: Mean gradients (fire emission rates), in g NO_x s^{-1} MW^{-1}, for each land cover type and the selected regions for MODIS Terra FRP vs. GOME-2 (left) and MODIS Aqua FRP vs. OMI (right). Only pixels with r > 0.3 and population density < 100 persons km^{-2} are included in the analysis

land cover type	global	ANE	ASE	CSA	NAU	SEA
1 broadleaf evergreen forest	**1.12 / 1.83**	1.37 / 2.91	-	1.18 / 1.72	-	0.74 / 2.15
2 coniferous evergreen forest	**1.08 /1.92**	-	-	-	-	-
3 high latitude deciduous forest	**1.13 / 2.10**	-	-	-	-	-
4 tundra	**0.55 / -**	-	-	-	-	-
5 mixed coniferous forest	**0.96 / 4.97**	-	-	-	-	-
6 wooded grassland	**1.21 / 3.22**	1.37 / 4.26	1.44 / 4.97	0.83 / 1.43	-	2.19 / 2.57
7 grassland	**0.77 / 2.11**	0.77 / 2.38	0.86 / 2.41	-	0.69 / 1.23	-
8 bare ground	**0.73 / 0.76**	-	-	-	-	-
9 shrubs and bare ground	**0.57 / 1.28**	-	0.67 / 1.24	-	0.60 / 1.34	-
10 cultivated crops	**1.14 / 2.57**	0.95 / 3.61	1.54 / 3.52	0.77 / 0.70	-	-
11 broadleaf deciduous forest	**1.03 / 1.77**	1.27 / 3.58	1.27 / 3.42	0.76 / 1.18	-	-

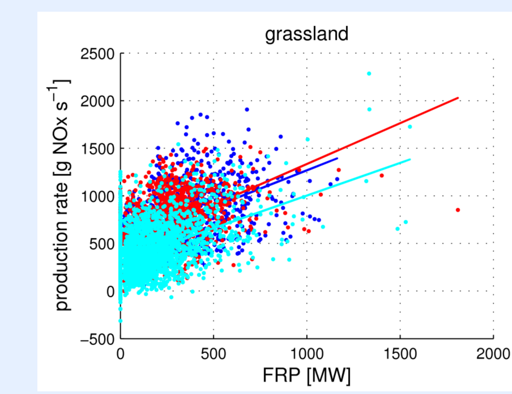

Fig. 8: Mean TVC (NO_2) FRP gradients (FERs) for grassland and wooded grassland within ANE (blue), ASE (red), CSA (green), NAU (turquois), and SEA (yellow). Data are shown for MODIS Terra FRP vs. GOME-2 TVC NO_2

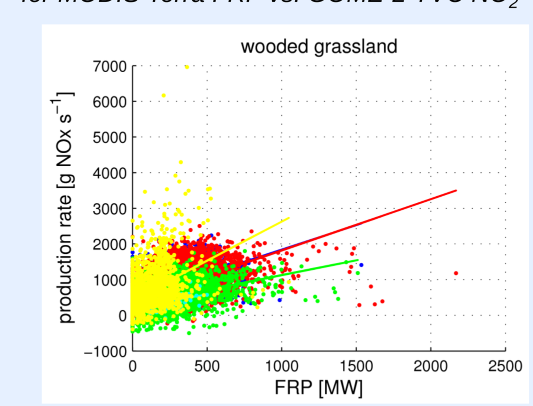

Conclusions

- The strong correlation between the two independent geophysical parameters FRP and TVC NO_2 has been investigated for the morning and early afternoon conditions
- After the conversion of TVC NO_2 into mass concentrations of NO_x, the use of a population density data set and a global land cover map enabled the estimation of fire emission rates of NO_x for different types of vegetation on a 1° x 1° grid
- The main results show that the highest FERs are found for wooded grassland, whereas the lowest values are found for tundra. Further, we found differences amongst the selected regions for certain land cover types (e.g. cultivated crops)
- Future work will be undertaken in order to enable the estimation of global fire emissions of NO_x by using the retrieved FERs

Acknowledgements

- GOME-2 lv1 data have been provided by EUMETSAT
- OMI lv2 data were provided by: http://disc.sci.gsfc.nasa.gov/Aura/data-holdings/OMI/omno2_v003.shtml
- MODIS data have been retrieved from: ftp://neespi.gsfc.nasa.gov/data/s4pa/Fire/
- population density was infered from: http://sedac.ciesin.columbia.edu/data/collection/gpw-v3
- global land cover classification was provided by: http://glcf.umd.edu/data/landcover/
- S. F. Schreier gratefully acknowledges funding by the ESSReS

Selected references

DeFries R.S. and Townshend J.R.G., in International Journal of Remote Sensing, 15:17, 3567-3586, 1994

Justice C.O. et al., in Remote Sensing of Environment, 83, 244-262, 2002

Richter A. and Burrows J.P., in Advances in Space Research, 29:11, 1673-1683, 2002

Callies J. et al., in Proceedings of SPIE, 5549 , art. no. 07 , 60-70, 2004

Bucsela E.J. et al., in IEEE Transactions on Geoscience and Remote Sensing, 44, 1245-1258, 2006

Wang P. et al., in Atmospheric Chemistry and Physics, 8, 6565-6576, 2008

Richter A. et al., in Atmospheric Measurement Techniques, 4, 1147–1159, 2011

Universität Bremen

www.iup.uni-bremen.de/doas

www.earth-system-science.org